Am J Transl Res 2023;15(7):4558-4572
www.ajtr.org /ISSN:1943-8141/AJTR0149918

Original Article

Peptidyl arginine deiminase inhibition alleviates angiotensin II-induced fibrosis

Takeshi Ijichi[1,2], Niveda Sundararaman[1,3], Thomas G Martin[4], Rakhi Pandey[1,3], Etai Koronyo[1,3], Jonathan A Kirk[4], Eduardo Marbán[1], Jennifer E Van Eyk[1,3], Justyna Fert-Bober[1,3]

[1]Smidt Heart Institute, Cedars-Sinai Medical Center, Los Angeles, CA 90048, The United States; [2]Department of Cardiology, School of Medicine, Tokai University, Isehara, Kanagawa 259-1193, Japan; [3]Advanced Clinical Biosystems Research Institute, Cedars-Sinai Medical Center, Los Angeles, CA 90048, The United States; [4]Department of Cell and Molecular Physiology, Loyola University Chicago Stritch School of Medicine, Maywood, IL 60153, The United States

Received March 1, 2023; Accepted June 14, 2023; Epub July 15, 2023; Published July 30, 2023

Abstract: Objectives: The conversion of protein arginine residues to citrulline by calcium-dependent peptidyl arginine deiminases (PADs) has been implicated in the pathogenesis of several diseases, indicating that PADs are therapeutic targets. A recent study indicated that PAD4 regulates age-related organ fibrosis and dysfunction; however, the specific role of this PAD and its citrullination substrate remains unclear. We investigated whether pharmacological inhibition of PAD activity could affect the progression of fibrosis and restore heart function. Methods: Cardiac hypertrophy was induced by chronic infusion of angiotensin (Ang) II. After 2 weeks of AngII infusion, a PAD inhibitor (Cl-amidine hydrochloride) or vehicle (saline) was injected every other day for the next 14 days together with the continued administration of AngII for a total of up to 28 days. Cardiac fibrosis and remodeling were evaluated by quantitative heart tissue histology, echocardiography, and mass spectrometry. Results: A reverse AngII-induced effect was observed in PAD inhibitor-treated mice (n=6) compared with AngII vehicle-treated mice, as indicated by a significant reduction in the heart/body ratio (AngII: 6.51±0.8 mg/g vs. Cl-amidine: 5.27±0.6 mg/g), a reduction in fibrosis (AngII: 2.1-fold increased vs. Cl-amidine: 1.8-fold increased), and a reduction in left ventricular posterior wall diastole (LWVPd) (AngII: 1.1±0.04 vs. Cl-amidine: 0.78±0.02 mm). Label-free quantitative proteomics analysis of heart tissue indicated that proteins involved in fibrosis (e.g., periostin), cytoskeleton organization (e.g., transgelin), and remodeling (e.g., myosin light chain, carbonic anhydrase) were normalized by Cl-amidine treatment. Conclusion: Our findings demonstrate that pharmacological inhibition of PAD may be an effective strategy to attenuate cardiac fibrosis.

Keywords: Peptidyl arginine deiminase (PAD), PAD inhibitor, cardiac fibrosis, proteomics, mass spectrometry

Introduction

Fibrosis begins as an intrinsic response to injury or aging and protects tissue from further damage [1, 2]. Cardiac fibrosis results from activated cardiac myofibroblasts, which secrete extracellular matrix (ECM) proteins in an effort to replace damaged tissue; however, prolonged and excessive ECM deposition leads to pathological fibrotic remodeling [3] that impairs cardiac compliance due to ventricular wall stiffening [4, 5] and disrupts electrical transmission between cardiomyocytes [6, 7]. Thus, fibrosis ultimately leads to adverse outcomes such as heart failure (HF) with increased mortality [8]. Despite its clinical and pathophysiological significance, no interventions or targeted therapies can currently mitigate or reverse cardiac fibrosis. Peptidyl arginine deiminases (PADs) belong to a family of hydrolases that mediate posttranslational modifications of arginine (Arg, R) within proteins to the amino acid citrulline in a calcium-dependent manner [9], which is a process called citrullination. PAD4 is necessary for chromatin decondensation during neutrophil extracellular trap (NET) formation [10]. Accordingly, PAD4-deficient mice were shown to lack NETosis, resulting in significant protection against acute tissue damage after ischemia and reperfusion [11, 12]. A recent

study demonstrated that, in addition to neutrophils, monocytes are rapidly recruited after ischemia onset [13]. In general, at early times and peaking at approximately day 3, neutrophils persist in the infarcted myocardium up to day 7 [14], and myocardial macrophages exhibit a change in their phenotype from M1 (1-3 days post-MI) to M2 (up to day 7) [13, 15]. Interestingly, monocyte/macrophage polarization has also been linked to PADs and shifts in PAD inform [16]. However, the relevance of citrullinated proteins and PADs in conditions other than acute myocardial injury remains unclear. Recent evidence has implicated angiotensin II (AngII) in the progression of myocardial fibrosis. AngII has been suggested to be a potent profibrotic molecule [17]. Increased serum levels of AngII were reported in patients with cardiovascular diseases that are associated with myocardial fibrosis, cardiac hypertrophy, and HF [18, 19]. Notably, extensive clinical and experimental evidence supports the protective effect of angiotensin converting enzyme inhibitors (ACEIs) and AngII type 1 receptor blockers against cardiac fibrosis [20]; however, whether established cardiac fibrosis in vivo can be reversed remains unclear. Therefore, the aim of the present study was to examine the involvement of citrullinated proteins and PADs in a murine model of cardiac fibrosis using a PAD inhibitor after the acute phase of injury. We hypothesize that inhibiting PAD activity in pronounced AngII-induced cardiac fibrosis will reverse cardiac fibrosis progression and improve cardiac function.

Materials and methods

The detailed and expanded methodology is provided in the online-only Supplementary Materials.

The following reagents were purchased: AngII (Sigma, cat. # A9525, St. Louis, MO), Cl-amidine (Cayman Chemical, cat. # 10599, Ann Arbor, MI), and LysC (Wako Chemicals, cat. # NC-9223464, Richmond, VA). All other chemicals were purchased from Fisher Scientific Co. (Hanover Park, IL).

Ethics statement

All experimental procedures followed the applicable principles set forth in the National Institutes of Health 2011 Guide for the Care and Use of Laboratory Animals. This study was approved by the Cedars-Sinai Medical Center Animal Care and Use Committee on Laboratory Animals.

Experimental groups

Male 8-10-week-old wild-type C57BL/6 mice (The Jackson Laboratory, Bar Harbor, ME) were housed in groups of 3-4 mice per cage, maintained under standard specific pathogen-free conditions, and given food and water ad libitum on 14 hr light/10 hr dark cycles at 21±2°C. After a 1-week acclimation period (T0), the mice were administered AngII (1.4 mg/kg/day) (Sigma-Aldrich, St. Louis, MO, USA) or an equivalent volume of sterile normal saline (sham group) using osmotic mini-pumps (Alzet, Cupertino model 1004, CA, USA) for 28 days to induce cardiac fibrosis as previously reported [21]. After the first 14 days of AngII infusion, the mice were administered Cl-amidine (10 mg/kg/day, Cayman Chemical, Ann Arbor, Mich., USA) or an equivalent volume of sterile normal saline (vehicle) every other day by subcutaneous injection for the next 14 days as previously described in parallel with the continuous administration of AngII [22]. At the end of the experiment (T28), the mice were humanely euthanized by decapitation under isoflurane anesthesia, and the hearts were harvested.

Echocardiography

Cardiac function and morphology were assessed under general anesthesia by transthoracic two-dimensional echocardiography using a Vevo 770 (VisualSonics, Toronto, Canada). Echocardiographic studies were performed at baseline before pump implantation (day 0) and after day 28 (n=5-7 per group). Anesthesia was induced with 3% isoflurane in oxygen and maintained at 1-2% during the procedure, and the heart rate was maintained at 450-550 beats per minute. The left atrial diameter, left ventricular internal diameter (LVID) at diastole and systole, left ventricular anterior wall (LVAW) thickness at diastole and systole, left ventricular posterior wall (LVPW) thickness at diastole and systole, left ventricular ejection fraction (EF%), and left ventricular fractional shortening (FS%) were analyzed as previously described [21, 23]. Diastolic wall strain (DWS), which is a noninvasive measure of left ventricular (LV) stiffness, was calculated as follows: DWS =

(LVPWs-LVPWd)/LVPWs, where LVPWs is the left ventricular posterior wall thickness at end-systole and LVPWd is the left ventricular posterior wall thickness at end-diastole, and end-diastolic and end-systolic measurements were made according to ASE recommendations [24]. EF% and FS% were calculated as follows: 100 × ([LVEDV-LVESV]/LVEDV) (%) and 100 × ([LVDd-LVDs]/LVDd) (%).

Determination of the heart weight/body weight (HW/BW) index

The BW of each mouse was measured before the animals were sacrificed. The weight of the whole heart (without heart auricles, the pericardium, and blood) was determined after carefully explanting the organ from the thorax and rinsing the organ thoroughly with PBS to remove any remaining blood. The index was calculated in mg HW/g BW.

Assessment of cardiac morphology

The excised hearts were cut at the midline into transverse blocks and embedded in a 10% formalin-PBS solution. Five-micrometer-thick paraffin-embedded sections were stained with Masson's trichrome solutions. Images were captured using a Pathscan Enabler IV scanner (Meyer Instruments, Houston, TX), and the cross-sectional area of cardiomyocytes was determined in the LV wall by tracing the boundaries of the cells using ImageJ software. Digital images were taken at 200× magnification in more than 20 random fields in each heart sample. Morphometric evaluation included the quantification of infarct wall thickness and non-infarcted remote wall thickness. Six to 10 sections per heart and 5 hearts in each group were analyzed and averaged.

Skinned myocytes

Tissue from the endocardium of the LV lateral wall was flash-frozen in liquid nitrogen and stored at -80°C. Functional experiments of isolated skinned myocytes were carried out as previously described [25, 26]. Briefly, the biopsies were incubated with 0.3% Triton X-100 buffer with protease inhibitors (Sigma-Aldrich, St. Louis, MO) and phosphatase inhibitors (PhosSTOP, Roche Applied Science, Penzberg, Germany) and then homogenized by low-speed pulverization to generate a skinned myocyte preparation. After being washed in isolation buffer, the myocytes were attached to a force transducer and motor arm. The force was measured as the bath Ca^{2+} concentration was increased from 0 to saturating conditions (46.8 μM). The force-calcium data were fit to the Hill equation: F = Fmax × Cah/(ECh50 + Cah), yielding Fmax, calcium sensitivity (Ca^{2+} required to achieve 50% maximal force; EC50), and cooperativity (Hill coefficient, h).

Protein extraction

Snap-frozen LV heart tissues were ground in liquid nitrogen and homogenized in 100 mM Tris-Cl (pH 7.4), 2% SDS, 50 mM DTT, 5 mg/ml aprotinin, 5 mg/ml leupeptin, 5 mg/ml pepstatin A and 2 mM PMSF (500 μL homogenization buffer/100 μg tissue). The homogenates were repeatedly frozen/boiled and centrifuged at 13,000×g for 20 min at room temperature. The protein concentration of the collected supernatant was assayed with Pierce 660 nm protein assay reagent (Fisher Scientific Co.) and stored in aliquots of 200 μg at -80°C until use.

MS-based proteomics

Protein extracts (100 μg) from LV tissue were processed by the FASP protocol using Microcon 30k centrifugal ultrafiltration units (Merck, Darmstadt) according to the manufacturer's instructions. For digestion, LysC (Wako Chemicals, Richmond, VA, USA) in 50 mM Tris HCl buffer was added to each sample at an enzyme-to-final protein ratio of 1:30. We used data-dependent acquisition (DDA) and data-independent acquisition (DIA) for peptide detection and protein identification. To generate a peptide spectral library for the subsequent identification and quantification of peptides and proteins, peptides from representative specimens were pooled as previously described [26]. These samples were analyzed by DDA mass spectrometry (MS) to assemble a hypercitrullinated mouse LV peptide assay library. Peptide peak groups were extracted from an existing library of pooled mouse LV lysates as described previously [27] and used for the SWATH workflow (DIA acquisitions) (see the Supplementary Materials for the detailed method section).

Statistical analysis

The results are expressed as mean ± SEM. Groups were compared using 1-way ANOVA followed by Tukey's multiple comparison post hoc

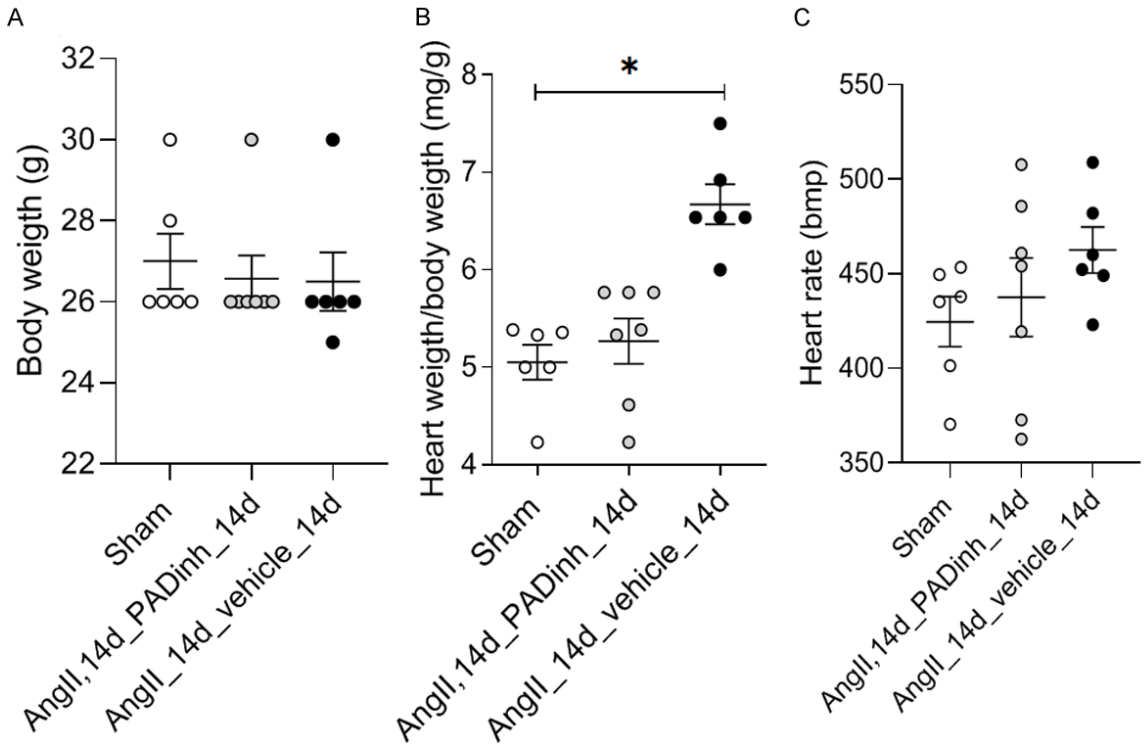

Figure 1. Cl-amidine treatment alleviated AngII-induced cardiac morphological remodeling. (A) Quantification of HW, (B) HW/BW ratio, and (C) heart rate. The results are expressed as the mean ± SEM; n=6-7 animal/group, *P < 0.05.

analysis. Comparisons between time points within the same group were performed by paired Student's two-tailed t test. Comparisons between two groups were performed by unpaired Student's two-tailed t test with Welsh's correction. Statistical analysis of histopathologic grading was performed using the nonparametric Kruskal-Wallis test. A p value < 0.05 was taken to indicate statistical significance. MS data were analyzed using MapDia for normalization, fragment/peptide selection, and statistical modeling [28]. All data were log2 transformed, and the differences in protein levels were compared by Welch's t test with Benjamini's-Hochberg's corporation of p value [29]. All the identified differentially expressed proteins were subjected to protein pathway analysis using the Ingenuity Pathway Analysis (IPA) tool (http://www.ingenuity.com) and a graphical tool for gene enrichment analysis (ShinyGO) 0.76.1 (http://bioinformatics.sdstate.edu) [30]. Enriched biological pathways in the mouse samples were identified by querying the list of significant proteins in the online Kyoto Encyclopedia of Genes and Genomes (KEGG) database against the background of all genes available in the database.

Results

Inhibiting PAD activity improved AngII-induced cardiac morphological remodeling

The BW, BW/HW ratio and heart rate were measured in the mice. BW was essentially unchanged in all groups (**Figure 1A**); however, HW was significantly increased in the AngII_14d_vehicle_14d group (**Figure 1B**). Mice that were treated with the PAD inhibitor after 14 days of AngII infusion had a slight but not significant increase in heart weight compared to sham mice but lighter hearts than AngII_14d_vehicle_14-treated mice (**Figure 1B**). The heart rate was increased in the AngII_14d_vehicle_14d group, but the difference was not significant (**Figure 1C**).

Inhibiting PAD activity improved cardiac functional remodeling in AngII-treated mice

The echocardiographic examination showed that the left ventricular dimensions, such as diastolic interventricular septum thickness (IVSd), systolic interventricular septum thickness (IVSs), diastolic left ventricular posterior

wall depth (LVPWd) and systolic left ventricular posterior wall thickness (LVPWs), were significantly increased after 28 days of AngII infusion compared to those in the sham group (1.13±0.04 vs. 0.73±0.03 mm, P < 0.01, 1.66± 0.07 vs. 1.24±0.08, 1.14±0.04 vs. 0.72±0.04, 1.51±0.01 vs. 1.17±0.09; n=5-7, respectively) (**Table 1**). Animals that were treated with intraperitoneal injections of Cl-amidine and continuous administration of AngII exhibited reductions in ventricular dimensions, including LVPWd (0.78±0.02 vs. 1.14±0.04 mm), LVWPs (1.30±0.07 vs. 1.51±0.03), IVSd (0.79±0.03 vs. 1.13±0.04) and IVSs (1.34±0.04 vs. 1.66± 0.07), compared to AngII vehicle-treated mice (**Table 1**). Furthermore, Cl-amidine normalized the E/A ratio in the AngII-treated group (1.23±0.10 vs. AngII_14d_vehicle_14d: 1.60± 0.080; P < 0.05) (**Table 1** and Supplementary Figure 2). No improvements in LV shortening or LV ejection fraction were observed in the Cl-amidine group, suggesting that myocardial contractility and heart function itself were not compromised at the time of the experiment, which was probably due to the young age of the mice (**Table 1**).

Inhibiting PAD activity alleviated AngII-induced cardiac fibrosis

Heart sections were stained with Masson's trichrome and examined by light microscopy (**Figure 2A**). Cardiomyocyte size was examined by determining the cross-sectional area and was increased in mice infused with AngII compared to sham mice (**Figure 2B**). There was no difference in cardiomyocyte size between the vehicle- and Cl-amidine-treated groups. Interstitial fibrotic areas were stained with blue dye and quantitatively determined (**Figure 2C**). The fibrotic areas were increased after 28 days of AngII infusion (6.8±0.3%) compared with those in the sham group (4.0±0.24%; P < 0.0001; n=5-6); this increase was attenuated by Cl-amidine treatment (4.6±0.54%, P < 0.001) (**Figure 2D**).

Inhibiting PAD activity attenuated quantitative changes in protein expression

To elucidate the molecular mechanisms by which PAD modulates fibrosis, we sought to identify the changes in proteins and citrullinated proteins in heart tissue. MS-based analysis identified a total of 1427 unambiguous proteins in the LysC digestion with high confidence. A heatmap of hierarchical clustering analysis (**Figure 3A**), a bar diagram (**Figure 3B**), and a Venn diagram (**Figure 3C**) were constructed to present an overall view of the proteomics data. By default, a 1.5-fold change threshold (i.e., log2FC ≥ 0.6 or log2FC ≤ -0.6) and a *p* value (false discovery rate, FDR) threshold of < 0.05 were applied. Compared with the sham group, the AngII_14d_vehicle_14d group had 147 differentially expressed proteins, including 108 upregulated and 39 downregulated proteins (**Figure 3B**). Thirty-seven of these proteins met the criteria of log2FC < ± 0.6 and *p* value (Supplementary Table 1, blue). A total of 240 differentially expressed proteins were identified in the AngII_14d_PADinh_14d group, of which 65 had higher abundance and 175 had lower abundance than in the AngII_14d_vehicle_14d group (**Figure 3C** and Supplementary Table 1). Eighteen of these proteins met the criteria of log2FC < ±0.6 and *p* value (0.05) (Supplementary Table 1, blue). Many proteins that had altered expression in the AngII_14d_vehicle_14d group compared to the sham group corresponded to previously reported changes in genes and/or proteins in end-stage HF and fibrosis, including elevated myosin light chain 1 (Myl1) [31], calponin-1 (CNN1) [32], periostin (POSTN) [33], transgelin (TAGL) [34], fatty acid synthase (FAS) [35], four and a half LIM domains protein 1 (FHL1) [36], and cofilin-1 (COF1) [37], among others (**Table 2**). Notably, many of those proteins were normalized by PAD inhibitor treatment, including POST, filamin-A (FLNA), galectin-3 (LEG3), and TAGL (**Table 2**). Interestingly, we identified 47 upregulated proteins (4 significant) in the PAD inhibitor treatment group compared to the sham group. Only one protein was downregulated when the AngII_14d_PADinh_14d group was compared to the sham group. The significantly upregulated proteins included D-beta-hydroxybutyrate dehydrogenase (BDH), myosin 7 (MYH7), lactadherin (MFGM), and actin alpha skeletal muscle (ACTS) (Supplementary Table 1).

Next, we focused on identifying citrullinated proteins. In total, we detected and identified 157 citrullinated residues in 92 proteins (Supplementary Table 2). Several proteins contained more than 1 citrullinated peptide, including myosin-6 (Myh6), which had 10 citrullinated peptides (16 unique sites); titin (TITIN),

Table 1. Echocardiographic parameters of the experimental animal model and treatment

Echocardiographic parameters	Sham_group (T0)	Sham_group (T28)	AngII_14d_PADinh_14d (T0)	AngII_14d_PADinh_14d (T28)	AngII_14d_vehicle_14d (T0)	AngII_14d_vehicle_14d (T28)
IVSd, mm	0.71±0.02	0.73±0.02	0.76±0.02	0.79±0.03 (+)	0.77±0.04	1.13±0.04 (**)
IVSs, mm	1.24±0.03	1.24±0.08	1.31±0.05	1.33±0.05	1.34±0.04	1.66±0.07
LVDd, mm	21.10±0.61	23.04±0.62	20.97±0.52	21.25±0.74	21.97±1.07	17.31±1.23
LVPWd, mm	0.73±0.01	0.72±0.04	0.77±0.02	0.78±0.02 (+)	0.76±0.03	1.14±0.04 (**)
LVPWs, mm	1.30±0.06	1.17±0.09	1.30±0.06	1.30±0.07 (+)	1.26±0.05	1.51±0.03 (**)
LVIDd, mm	3.53±0.10	4.04±0.1	3.5±0.1	3.68±0.11	3.78±0.08	3.38±0.11 (*)
LVIDs, mm	2.14±0.06	2.81±0.22	2.11±0.11	2.33±0.16	2.46±0.11	2.11±0.13
FS, %	39.25±1.71	36.27±2.07	39.69±2.46	37.16±2.86	35.12±2.37	36.56±2.56
EF, %	58.56±1.75	55.4±1.56	59.20±1.07	55.91±1.17	60.95±1.55	55.91±1.44
E/A' ratio	1.15±0.02	1.37±0.08	1.1±0.03	1.23±0.02 (+)	1.16±0.02	1.60±0.05 (*)
E/e ratio	23±1.66	23.58±0.75	24.21±1.94	31.14±2.92 (++)	25.1±1.91	29.17±2.60 (*)

LVPWs, left ventricular posterior wall, systole; LVPWd, left ventricular posterior wall, diastole; IVSs, intraventricular septum, systole; IVSd, intraventricular septum, diastole; HR, heart rate; EF, ejection fraction; FS, fractional shortening; E, A, wave velocity; E', A', tissue Doppler wave; *p* value of *P < 0.05, **P < 0.01 when AngII_14d_vehicle_14d was compared to sham, *p* value of +P < 0.05, ++P < 0.01 when AngII_14d_PADinh_14d was compared to sham.

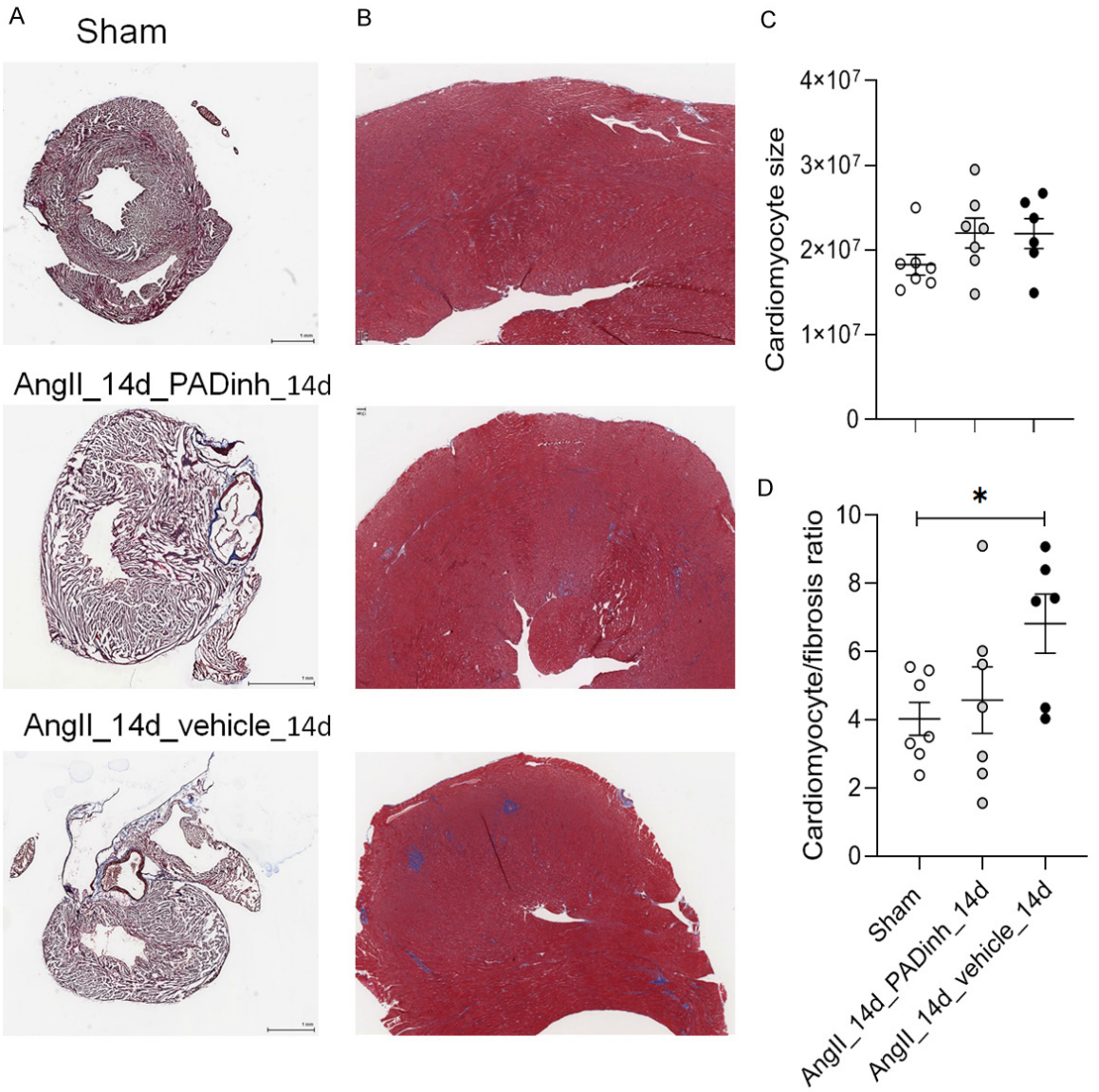

Figure 2. Immunohistochemistry of cardiac sections. A. Micrographs (magnification: ×4) showing the representative cross-sectional area of heart sections stained with Masson trichrome from mice that received a subcutaneous infusion of saline or AngII for 28 d treated with vehicle or PAD inhibitor for 14 d. Scale bars, 1 mm. B. Micrographs showing interstitial left ventricular (LV) fibrosis in myocardial sections stained with Masson trichrome at higher magnification. C. Cardiomyocyte size in the section of the left ventricular end posterior wall (LVPW) was determined from the cross-sectional area. D. Blue-stained interstitial fibrotic areas in the sections were quantitatively determined. The results are expressed as the mean ± SEM; n=6-7 animals/group, *P < 0.05, **P < 0.01.

which had 7 citrullinated peptides (7 unique sites); aconitate hydratase (ACON), which had 9 citrullinated peptides (9 unique sites); and ATP synthase subunit alpha (ATPA), which had 3 citrullinated peptides (3 unique sites) (Supplementary Table 2). Citrullinated peptides were filtered using a moderated t test, and peptides that had a 1.5-fold change (log2FC) ≤ -0.6 or ≥ 0.6 and *p* value < 0.05 were considered significant (**Table 3**). Compared with the sham group, the AngII_14d_vehicle_14d group had 23 upregulated citrullinated peptides (4 significant) and 12 downregulated citrullinated residues (1 significant). In contrast, when comparing the AngII_14d_vehicle_14d group to the AngII_14d_PADinh_14d group, 16 citrullinated peptides were upregulated (1 significant), and 19 were downregulated (1 significant) (**Table 3**).

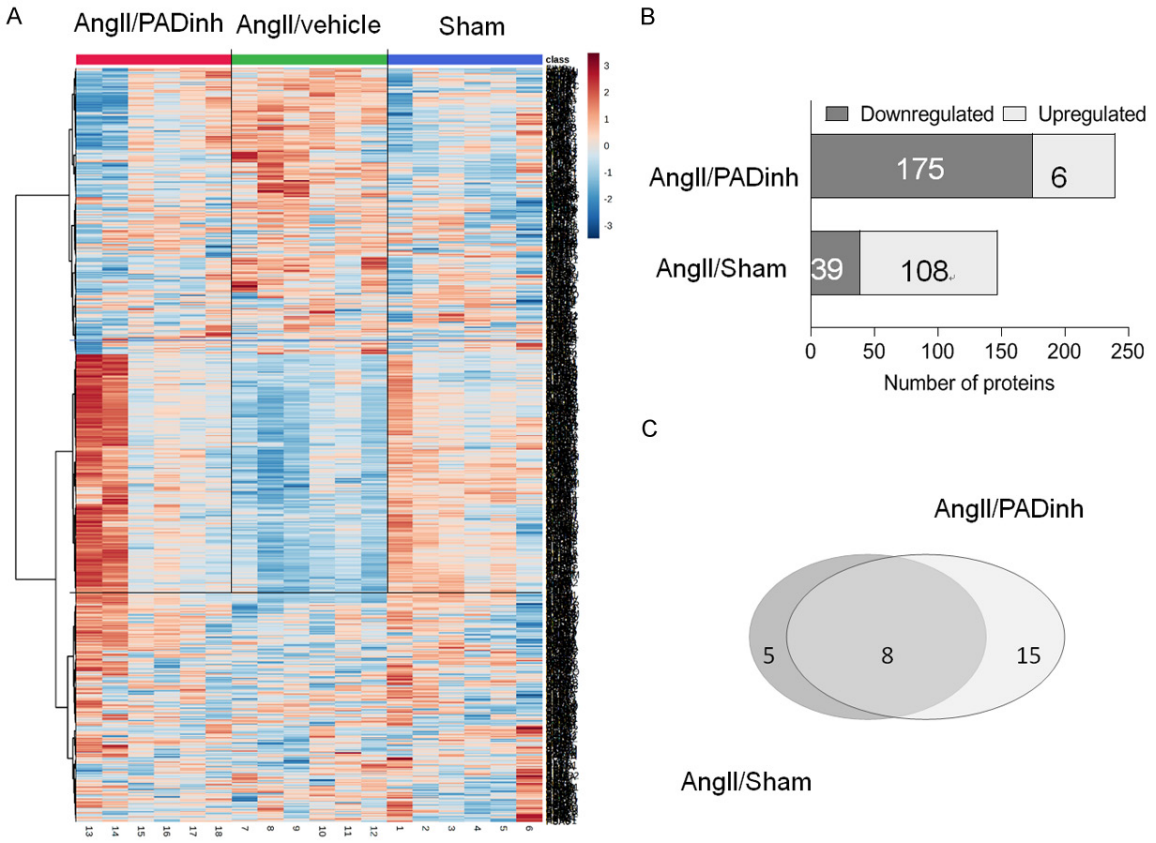

Figure 3. Overview of the proteomics results. A. Hierarchical clustering heatmap showing the proteomics results of 1427 identified proteins. Groups are presented as colors: red, AngII_14d_PAD-inh_14d; blue, Sham; green, AngII_14d_vehicle_14d. B. Bar diagrams showing differentially expressed proteins that met the criteria 1 > peptide identified, log2FC ≥ 0.6 or log2FC ≤ -0.6 comparing the AngII_14d_vehicle_14 group to the sham group (lower) and the AngII_14d_vehicle_14 group to the AngII_14d_PADinh_14d group (upper). C. Venn diagram showing the overlap of quantified proteins in the compared groups, which were expressed as AngII-14d_vehicle_14d group to the sham group (left) and to the AngII_14d_PADinh_14d group (right).

Gene Ontology (GO) analyses were performed using the shared (**Figure 4**) or distinctive differentially expressed proteins (**Figure 5**), and the top-ranked terms were biological process, molecular function, cellular component, and Kyoto Encyclopedia of Genes and Genomes (KEGG) pathways. The shared differentially expressed citrullinated peptides were mainly associated with cardiac muscle contraction, followed by metabolic and energy production processes (**Figure 4A-D**). In the distinctive analysis, differentially expressed citrullinated peptides were primarily related to the regulation of heart contraction (**Figure 5A-D**). Notably, several of the citrullinated proteins, including putative hydrolase (RBBP9), dihydrolipoamide succinyltransferase (OD02), acetyl-CoA acetyltransferase, myosin 6 (Myh6), mitochondrial (THIL), and heat shock protein 90-beta (HSP90), were associated with cardiac muscle hypertrophy and were downregulated by PAD inhibitor treatment.

Discussion

Cardiac fibrosis is an important pathological process involved in most myocardial diseases. We previously demonstrated that the levels of citrullinated peptides were increased in the myocardium of human HF patients [26]. This finding raised the question of whether citrullination is an active player in cardiac fibrosis. The aim of this study was to investigate the effect and mechanism of PAD inhibition on cardiac fibrosis. Importantly, (1) we used an AngII-induced cardiac fibrosis mouse model because the complex interactions between ischemia and the development of fibrosis have been

Table 2. Heatmap of differentially expressed proteins in the AngII_14d_vehicle_14d, AngII_14d_PADinh_14d, and sham groups

Protein name	Biological terms	AngII_14d_vehicle_14d/Sham		AngII_14d_vehicle_14d/AngII_14d_PADinh_14d		AngII_14d_PADinh_14d/Sham	
		log2FC	*p* value	log2FC	*p* value	log2FC	*p* value
Acute-phase response							
Alpha-2-HS-glycoprotein	FETUA	0.809709	0.00	0.534289	1.69E-08	0.276558	0.50
Aging							
Angiotensin-converting enzyme	ACE	0.828255	4.54E-15	0.510349	2.80E-03	0.29547	9.14E-03
Eukaryotic translation elongation factor 1 alpha 1	EF1A1	0.44964	5.20E-06	0.65846	9.82E-11	-0.208609	0.78
Cell proliferation, migration							
Microsomal glutathione S-transferase 1	MGST1	0.736751	2.96E-05	1.06154	9.30E-14	-0.326118	0.41
Iq motif containing gtpase activating protein 1	IQGA1	0.776668	0.00	0.525869	1.04E-06	0.230734	0.73
Fibrosis/Cytoskeletal organization							
Collagen alpha-1 (XIV) chain	COEA1	0.488689	1.68E-03	0.337863	0.18	0.092515	0.62
Four and a half lim domains 1	FHL1	0.761195	0.00	0.412874	2.43E-03	0.317179	0.76
Fibrinogen alpha chain	FIBA	0.423595	2.11E-08	0.1523	0.79	0.23814	0.45
Filamin-A	FLNA	0.628524	0.00	0.289862	0.83	0.31358	1.15E-14
Galectin-3	LEG3	0.530539	2.01E-03	0.274352	0.39	0.256188	0.38
Periostin, osteoblast specific factor	POSTN	0.94061	0.00	0.265587	0.81	0.567123	0.32
Transgelin	TAGL	0.848858	0.00	0.432147	0.74	0.402907	9.27E-06
Transgelin-2	TAGL2	0.758486	0.00	0.539425	3.71E-09	0.212779	0.80
Metabolic process							
Carbonyl reductase [NADPH] 2	CBR2	1.84411	5.31E-10	2.4356	0.00E+00	-0.818763	0.20
Pyruvate carboxylase	PYC	0.89501	2.71E-13	0.701772	8.22E-05	0.305582	0.73
ATP-citrate synthase	ACLY	0.877413	1.16E-12	0.886863	1.19E-09	0.169603	0.78
Aldehyde dehydrogenase family 1	AL1A1	0.687177	1.46E-02	0.957772	6.49E-18	-0.214354	0.81
Transketolase	TKT	0.659171	1.33E-18	0.684599	1.17E-16	-0.04828	0.81
Dimethylaniline monooxygenase [N-oxide-forming] 2	FMO2	0.58489	4.19E-05	0.969108	4.29E-06	-0.383159	0.72
NADPH--cytochrome P450 reductase	NCPR	0.434563	0.27	0.60218	8.30E-04	-0.169484	0.74
Glycerol-3-phosphate dehydrogenase [NAD(+)]	GPDA	0.387725	0.81	0.714204	0.00	-0.30371	0.81
Fatty acid synthase	FAS	1.33787	0.00	0.993005	0.00	0.366123	0.80
Tricarboxylate transport protein, mitochondrial	TXTP	1.06308	1.17E-11	1.18787	1.95E-09	-0.127891	0.77
Muscle contraction							
Myosin light chain 1/3, skeletal muscle isoform	MYL1	1.11291	0.00	0.95327	0.00	0.0947365	0.82
Myosin, light polypeptide 3	MYL3	-0.2358	0.78	-0.619442	0.00	0.381989	0.00
Calponin-1	CNN1	0.837377	1.92E-10	0.495633	0.46	0.324316	4.90E-02
Response to stress							
Carbonic anhydrase 3	CAH3	0.96208	0.00	1.23807	0.00	-0.289776	0.82
Serine (or cysteine) peptidase inhibitor	A1AT5	0.489519	4.60E-07	0.714069	0.00	-0.19382	0.77

A pseudo heatmap was constructed from the comparisons of differentially expressed proteins in Supplementary Table 1 for the AngII_14d_vehicle_14d, AngII_14d_PADinh_14d, and sham groups. Related biological themes from the list of differentially expressed proteins were grouped into higher-level biological groupings to permit comparisons between the various AngII-treated subgroups (Key: red = increased expression; blue = decreased relative expression).

described previously [12, 38]; (2) young mice were used to exclude fibrosis processes related to aging; and (3) the delivery of a PAD inhibitor 14 days after chronic AngII infusion was performed to rescue but not prevent fibrosis. We showed that chronic AngII exposure resulted in positive staining for markers of fibrosis, including positive collagen staining, increased heart size (HW/BW ratio) and LV mass (IVSd, LVPWd). Our proteomics results confirmed the increase in the expression of proteins involved in fibrosis (POSTN, FLNA, LEG3, TAGL) and the cardiac hypertrophy response to stress contractile processes (Myl1, CNN1, FAS). Animals that were further treated with the PAD inhibitor showed a decrease in cardiac fibrosis and a decrease in the HW/BW ratio and LV mass. PAD inhibitor treatment had no effect on total collagen accumulation, as measured by quantitative histology (data not shown). However, the mass spec-

Table 3. Differentially expressed citrullinated proteins with corresponding citrullinated peptides and related biological processes and functions

UniProt ID	Name	Peptide	Citrullinated peptides				Total protein			
			AngII_14d_vector_14d vs. Sham		AngII_14d_vector_14d vs. AngII_14d_PADinh_14d		AngII_14d_ vehicle_14d/Sham		AngII_14d_vehicle_14d/ AngII_14d_PADinh_14d	
			Log2FC	FDR (*p* value)	Log2FC	FDR (*p* value)	Log2FC	FDR (*p* value)	Log2FC	FDR (*p* value)
P09103	PDIA1	RcitTGPAATTLSDTAAAESLVDSSEVTVIGFFK	2.634	0.0154	0.915	0.1470	0.340	0.0205	0.321	0.7141
Q91YQ5	RPN1	RcitTVDLSSHLAK	1.532	0.0267	1.095	0.0893	0.392	0.0821	0.354	0.5222
O88851	RBBP9	EQQEVADRcitLDAK	1.219	0.0213	-0.406	0.1872	0.252	0.4780	-0.481	0.0046
P01942	HBA	IGGHGAEYGAEALERcitMFASFPTTK	1.070	0.2919	0.837	0.3916	0.660	0.0000	0.428	0.0000
Q9D2G2	ODO2	AAVEDPRcitVLLLDL	1.030	0.2433	-0.674	0.2014	-0.083	0.7993	-0.304	0.0000
Q02566	MYH6	TTHPHFVRcitCIIPNERK	0.983	0.4194	-0.362	0.7249	-0.182	0.8306	-0.421	0.0000
Q8QZT1	THIL	MNISRQEQDTYALSSYTRcitSK	0.961	0.2266	-0.398	0.4059	-0.112	0.8219	-0.248	0.0000
P11499	HS90B	EQVANSAFVERcitVRK	0.961	0.3747	-0.713	0.2981	0.040	0.8212	-0.039	0.8222
P00920	CAH2	DFPIANGDRcitQSPVDIDTATAQHDPALQPLLISYDK	0.926	0.1806	0.499	0.4385	0.747	0.0000	0.502	0.0000
P09103	PDIA1	KEECPAVRcitLITLEEEMTK	0.802	0.3716	3.521	0.0470	0.340	0.0205	0.321	0.7141
P07724	ALBU	DDNPSLPPFERcitPEAEAM (UniMod_35) CTSFK	0.793	0.0420	0.523	0.1482	0.440	0.0000	0.283	0.8284
P68134	ACTS	DLYANdeamNVMSGGTTMYPGIADRcitMQK	0.790	0.1571	-0.597	0.0835	0.251	0.7750	-0.403	0.0000
Q9JI91	ACTN2	VIQSYSIRISSSNPYSTVTMDELRcitNK	0.788	0.4380	-0.612	0.3349	-0.123	0.8278	-0.416	0.0000
Q8VDD5	MYH9	DVDRcitIIGLDQdeamVAGMSETALPGAFK	0.764	0.1436	0.777	0.1356	0.455	0.0000	0.393	0.0000
Q9CZU6	CISY	LRcitDYIWNTLNSGRVVPGYGHAVLRK	0.725	0.5453	-0.457	0.5816	-0.186	0.7231	-0.278	0.0000
P08249	MDHM	NSPLVSRLTLYDIAHTPGVAADLSHIETRcitANVK	0.703	0.4811	-0.346	0.6309	-0.129	0.8274	-0.263	0.0000
P09541	MYL4	ESNGTVMGAELRcitHVLATLGEK	0.683	0.2006	0.804	0.1467	0.710	0.0000	0.147	0.0000
Q8BTM8	FLNA	YAVRFIPRcitENGIYLIDVK	0.652	0.1444	0.444	0.3994	0.629	0.0000	0.290	0.8273
P01837	IGKC	IDGSERcitQNGVLNSWTDQDSK	0.649	0.1237	0.470	0.2127	0.709	0.0000	0.531	0.0000
P27773	PDIA3	IFRDGEEAGAYDGPRcitTADGIVSHLK	0.639	0.1752	0.514	0.2479	0.372	0.0000	0.321	0.0000
P49312	ROA1	IEVIEIMTDRcitGSGK	0.613	0.4353	0.091	0.8905	0.047	0.7877	-0.016	0.7723
P05977	MYL1	EGNdeamGTVM (UniMod_35) GAELRcitHVLATLGEK	0.608	0.5163	0.926	0.3788	1.113	0.0000	0.953	0.0000
Q99KI0	ACON	NTIVTSYNRNFTGRcitNDANPETHAFVTSPEIVTALAIAGTLK	0.608	0.4560	-0.351	0.3920	-0.160	0.8295	-0.311	0.0000
Q60605	MYL6	DQGTYEDYVEGLRcitVFDK	-0.609	0.2437	-0.105	0.8919	0.569	0.0000	0.340	0.7251
Q8BWT1	THIM	QTM (UniMod_35) QVDEHARcitPQTTLEQLQK	-0.627	0.0681	-0.512	0.2715	-0.277	0.0000	-0.301	0.0000
P54071	IDHP	GRPTSTNPIASIFAWTRGLEHRcitGK	-0.650	0.0473	-0.080	0.9101	-0.247	0.0000	-0.468	0.0000
P24549	AL1A1	LADLMERcitDRLLLATMEALNGGK	-0.654	0.3812	-0.977	0.1483	0.687	0.0146	0.958	0.0000
Q99JY0	ECHB	AMDSDWFAQNYMGRcitK	-0.676	0.3669	-0.878	0.1457	-0.329	0.0000	-0.366	0.0000
Q9D6R2	IDH3A	RIAEFAFEYARNNHRcitSNVTAVHK	-0.717	0.4830	0.693	0.6346	-0.114	0.8165	-0.224	0.0000
Q9D6R2	IDH3A	RIAEFAFEYARcitNNHRSNVTAVHK	-0.726	0.4782	0.655	0.6550	-0.114	0.8165	-0.224	0.0000
Q9Z2I8	SUCB2	SENEPIENEAARcitYDLK	-0.817	0.1183	-0.984	0.0919	-0.201	0.8051	-0.318	0.0000
P07310	KCRM	AGHPFM (UniMod_35) WNEHLGYVLTCPSNLGTGLRcitGGVHVK	-0.864	0.1456	-1.202	0.0116	-0.167	0.8222	-0.409	0.0000
Q9WV92	E41L3	RcitSRcitGQVLFDK	-0.866	0.1583	-1.058	0.0884	-0.474	0.1372	-0.606	0.0059
P09542	MYL3	EGNdeamGTVMGAELRcitHVLATLGERLTEDEVEK	-1.024	0.1352	-1.583	0.0832	-0.236	0.7834	-0.619	0.0000
Q03265	ATPA	RTGAIVDVPVGEELLGRcitVVDALGNAIDGK	-1.228	0.3162	0.760	0.6033	-0.207	0.8075	-0.364	0.0000

Upregulated proteins are marked in red, and downregulated proteins are marked in blue. Rcit indicates a citrullinated residue, Ndeam indicates a deamidated residue, and Mox indicates an oxidated residue.

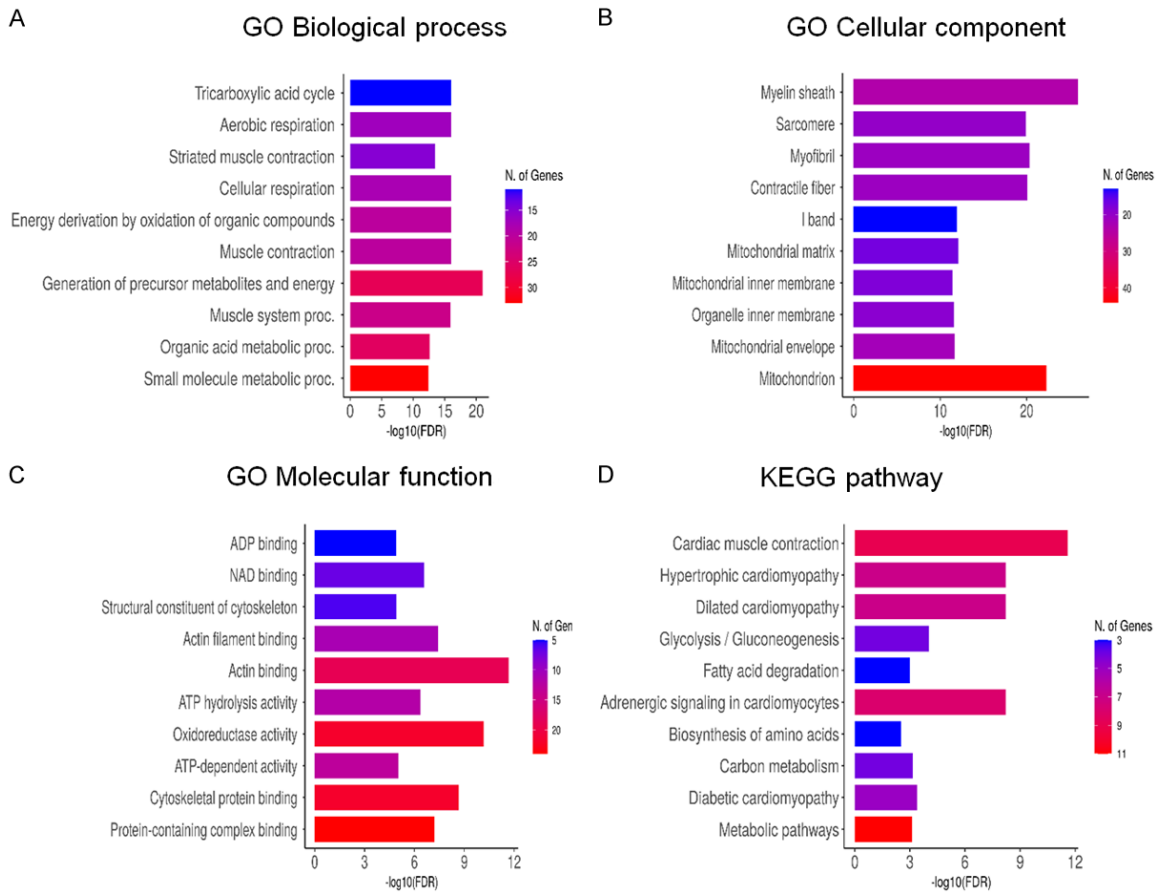

Figure 4. GO enrichment results showing the identified citrullinated proteins in terms of (A) biological process, (B) cellular component, (C) molecular function, and (D) KEGG pathway. Criteria: top 10 pathways, FDR 0.05, pathway size minimum 15 genes, x-axis represents -log10 FDR (*p* value), color represents number of genes per pathway.

trometry results showed that PAD inhibition suppressed other AngII-associated profibrotic markers, which ultimately could avert cardiac fibrosis, remodeling, and stiffness. The inhibition of PAD activity further affected metabolic pathways, including fatty acid degradation and the PRAR signaling pathway, which was followed by cardiac muscle contraction. In contrast, citrullinated peptides were predominantly associated with cardiac muscle contraction, and citrullinated proteins were involved in energy production processes. Notably, several proteins contained more than 1 citrullinated arginine residue, including Myh6 and titin. However, a reduction in citrullination did not correlate with improvements in heart contractility (EF%, ES%) (**Table 1**) or skinned myocyte tension measurement (Supplementary Figure 1). One explanation is that arginine citrullination is a relatively long-lived posttranslational modification due to the absence of a characterized peptidyl citrulline iminotransferase, which suggests that these modifications may only be reversed through protein turnover.

In contrast, long-lived citrullinated residues could also promote fibrosis and remodeling by supporting cytoskeletal assembly. For example, FLNA is an actin-crosslinking protein with 2 N-terminal actin-binding domains and 24 immunoglobulin-like repeats. FLNA is mostly localized in the membrane cytoskeleton, where it regulates a variety of cytoskeleton-related processes, including receptor clustering and crosstalk among different receptors and the actin cytoskeleton. FLNA contains 1 citrullinated residue (R2391) in the C-terminus. Interestingly, citrullinated FLNA has been reported to be an autoantigen in rheumatoid arthritis [39, 40]. In our study, the level of citrullinated FLNA increased with chronic AngII infusion and was normalized to almost sham levels by PAD inhibi-

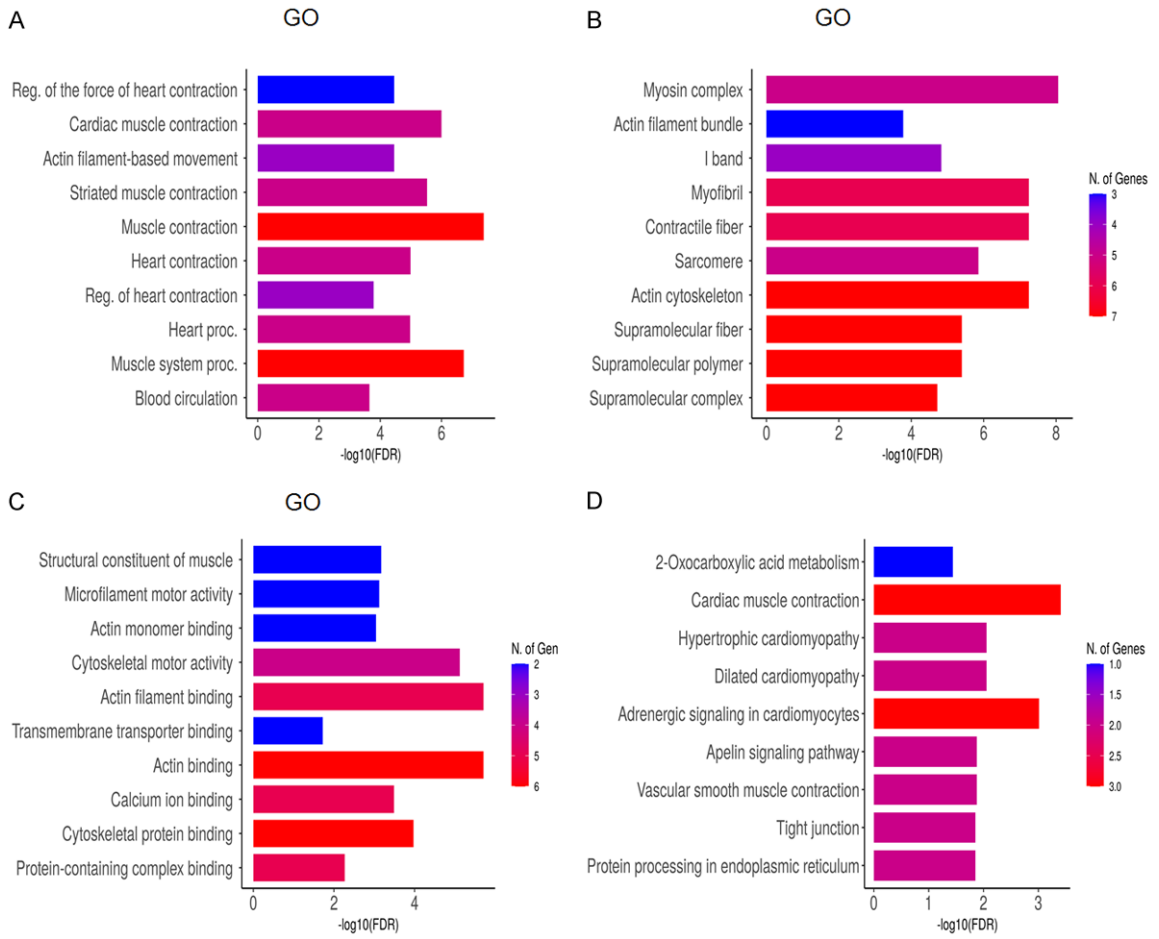

Figure 5. GO enrichment results showing the significantly differentially expressed proteins in terms of (A) biological process, (B) molecular function, (C) cellular component, and (D) KEGG pathway. Criteria: top 10 pathways, FDR 0.05, pathway size minimum 15 genes, x-axis represents -log10 FDR (*p* value), color represents number of genes per pathway.

tor injection (**Figure 6A**). Similarly, citrullination of ACTS, reported previously by us [26] and others [41], was increased in the AngII-14d_vehicle_14d group and was normalized by PAD inhibition (**Figure 6B**). Exploring the functional effect of citrullination on any of these proteins is very important; however, it is beyond the scope of this study. There are some potential limitations to this study. First, we used only young mice; aging leads to a more proinflammatory environment with higher numbers of neutrophils and NETosis [42-44] and age-related fibrosis [12]. Including only young mice allowed us to demonstrate that inhibiting PAD activity is beneficial in the absence of NETosis and age-related low-grade inflammation. Second, our proteomics data were focused only on citrullinated proteins; therefore, any crosstalk between PTMs could not be discussed in this manuscript. Despite these limitations, these results suggest that treatment with Cl-amidine reverses established cardiac fibrosis. Several citrullinated proteins have been identified, verifying that citrullination plays a critical role in numerous processes, such as fibrosis, remodeling, and cardiac energy metabolism; however, the exact role of each modified residue should be verified in an additional study in a larger cohort and the inclusion of sex- and age-dependent animals. Regardless, our results provide a rationale for the further development of intervention studies targeting PAD activity and citrullinated proteins.

Summary

In this study, we performed high-quality proteomics analysis of cardiac tissues from three

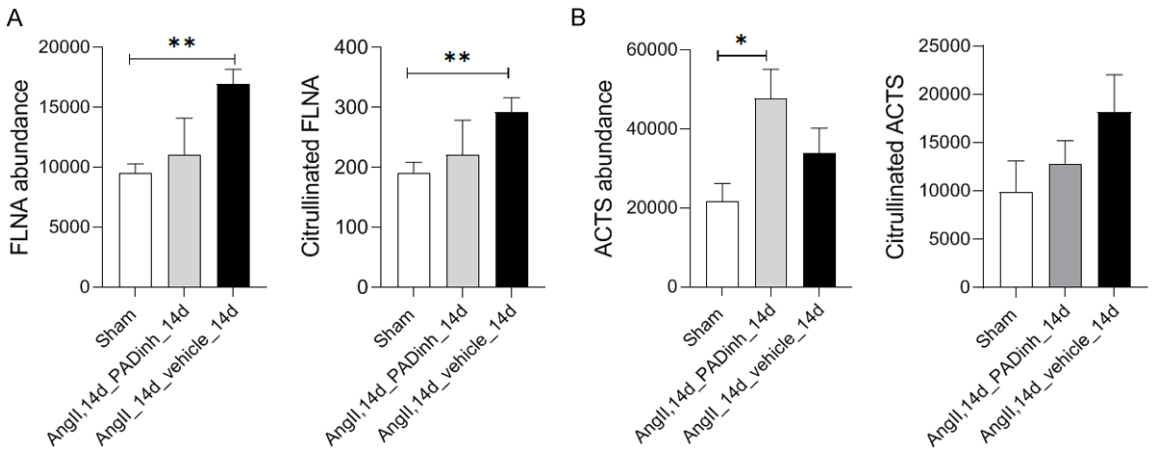

Figure 6. Differentially enriched citrullinated peptides in the AngII_14d_vehicle_14d group compared to the AngII_14d_PADinh_14d and sham groups identified using mass spectrometry. Normalized citrullinated peptide quantities of (A) FLNA (YAVRFIPR(2391)ENGIYLIDVK) and (B) ACTS (DLYANNVMSGGTTMYPGIADR(314)MQK), compared to the corresponding total protein expression. The results are expressed as the mean ± SEM; n=6-7 animals/group, *P < 0.05, **P < 0.01. Bold R with numbers in brackets corresponds to citrullinated residues in the protein sequence.

groups: a sham group and two AngII-induced cardiac fibrosis groups. The first group was treated with saline vehicle, and the second group was treated with the pharmacological PAD inhibitor Cl-amidine. We found several differentially expressed proteins and pathways between the groups. These proteins could be used as diagnostic and prognostic biomarkers. Additionally, we found several citrullinated peptides and proteins that could play major roles in cardiac fibrosis. Importantly, our study was a preliminary examination, and further experiments and validations are required to identify the role of differential citrullinated protein expression in cardiac fibrosis.

Acknowledgements

NIH 2R01HL136737 to JAK and AHA 20PRE-35170045 to TGM.

Disclosure of conflict of interest

The authors declare that this research was conducted in the absence of any commercial or financial relationships that could be construed as a potential conflict of interest.

Address correspondence to: Dr. Justyna Fert-Bober, Smidt Heart Institute, Cedars-Sinai Medical Center, 127 South San Vincente Blvd, AHSP A9229 Los Angeles, CA 90048, The United States. Tel: 424-315-2583; E-mail: Justyna.Fert-Bober@cshs.org

References

[1] Ivey MJ, Kuwabara JT, Pai JT, Moore RE, Sun Z and Tallquist MD. Resident fibroblast expansion during cardiac growth and remodeling. J Mol Cell Cardiol 2018; 114: 161-174.

[2] Piek A, de Boer RA and Silljé HH. The fibrosis-cell death axis in heart failure. Heart Fail Rev 2016; 21: 199-211.

[3] Valiente-Alandi I, Potter SJ, Salvador AM, Schafer AE, Schips T, Carrillo-Salinas F, Gibson AM, Nieman ML, Perkins C, Sargent MA, Huo J, Lorenz JN, DeFalco T, Molkentin JD, Alcaide P and Blaxall BC. Inhibiting fibronectin attenuates fibrosis and improves cardiac function in a model of heart failure. Circulation 2018; 138: 1236-1252.

[4] Tallquist MD and Molkentin JD. Redefining the identity of cardiac fibroblasts. Nat Rev Cardiol 2017; 14: 484-491.

[5] Frangogiannis NG. The extracellular matrix in ischemic and nonischemic heart failure. Circ Res 2019; 125: 117-146.

[6] Pellman J, Zhang J and Sheikh F. Myocyte-fibroblast communication in cardiac fibrosis and arrhythmias: mechanisms and model systems. J Mol Cell Cardiol 2016; 94: 22-31.

[7] Hall C, Gehmlich K, Denning C and Pavlovic D. Complex relationship between cardiac fibroblasts and cardiomyocytes in health and disease. J Am Heart Assoc 2021; 10: e019338.

[8] Mandawat A, Chattranukulchai P, Mandawat A, Blood AJ, Ambati S, Hayes B, Rehwald W, Kim HW, Heitner JF, Shah DJ and Klem I. Progression of myocardial fibrosis in nonischemic

DCM and association with mortality and heart failure outcomes. JACC Cardiovasc Imaging 2021; 14: 1338-1350.
[9] Anzilotti C, Pratesi F, Tommasi C and Migliorini P. Peptidylarginine deiminase 4 and citrullination in health and disease. Autoimmun Rev 2010; 9: 158-160.
[10] Leshner M, Wang S, Lewis C, Zheng H, Chen XA, Santy L and Wang Y. PAD4 mediated histone hypercitrullination induces heterochromatin decondensation and chromatin unfolding to form neutrophil extracellular trap-like structures. Front Immunol 2012; 3: 307.
[11] Eghbalzadeh K, Georgi L, Louis T, Zhao H, Keser U, Weber C, Mollenhauer M, Conforti A, Wahlers T and Paunel-Görgülü A. Compromised anti-inflammatory action of neutrophil extracellular traps in PAD4-deficient mice contributes to aggravated acute inflammation after myocardial infarction. Front Immunol 2019; 10: 2313.
[12] Martinod K, Witsch T, Erpenbeck L, Savchenko A, Hayashi H, Cherpokova D, Gallant M, Mauler M, Cifuni SM and Wagner DD. Peptidylarginine deiminase 4 promotes age-related organ fibrosis. J Exp Med 2017; 214: 439-458.
[13] Mouton AJ, DeLeon-Pennell KY, Gonzalez OJ, Flynn ER, Freeman TC, Saucerman JJ, Garrett MR, Ma Y, Harmancey R and Lindsey ML. Mapping macrophage polarization over the myocardial infarction time continuum. Basic Res Cardiol 2018; 113: 26.
[14] Ma Y, Yabluchanskiy A, Iyer RP, Cannon PL, Flynn ER, Jung M, Henry J, Cates CA, Deleon-Pennell KY and Lindsey ML. Temporal neutrophil polarization following myocardial infarction. Cardiovasc Res 2016; 110: 51-61.
[15] Yan X, Anzai A, Katsumata Y, Matsuhashi T, Ito K, Endo J, Yamamoto T, Takeshima A, Shinmura K, Shen W, Fukuda K and Sano M. Temporal dynamics of cardiac immune cell accumulation following acute myocardial infarction. J Mol Cell Cardiol 2013; 62: 24-35.
[16] Stachowicz A, Pandey R, Sundararaman N, Venkatraman V, Van Eyk JE and Fert-Bober J. Protein arginine deiminase 2 (PAD2) modulates the polarization of THP-1 macrophages to the anti-inflammatory M2 phenotype. J Inflamm (Lond) 2022; 19: 20.
[17] Sopel MJ, Rosin NL, Lee TD and Légaré JF. Myocardial fibrosis in response to angiotensin II is preceded by the recruitment of mesenchymal progenitor cells. Lab Invest 2011; 91: 565-578.
[18] Zhao Q, Ishibashi M, Hiasa K, Tan C, Takeshita A and Egashira K. Essential role of vascular endothelial growth factor in angiotensin II-induced vascular inflammation and remodeling. Hypertension 2004; 44: 264-270.
[19] Schnee JM and Hsueh WA. Angiotensin II, adhesion, and cardiac fibrosis. Cardiovasc Res 2000; 46: 264-268.
[20] Liu X, Shan X, Chen H, Li Z, Zhao P, Zhang C, Guo W, Xu M and Lu R. Stachydrine ameliorates cardiac fibrosis through inhibition of angiotensin II/transformation growth factor β1 fibrogenic axis. Front Pharmacol 2019; 10: 538.
[21] Cambier L, Giani JF, Liu W, Ijichi T, Echavez AK, Valle J and Marbán E. Angiotensin II-induced end-organ damage in mice is attenuated by human exosomes and by an exosomal Y RNA fragment. Hypertension 2018; 72: 370-380.
[22] Biron BM, Chung CS, O'Brien XM, Chen Y, Reichner JS and Ayala A. Cl-amidine prevents histone 3 citrullination and neutrophil extracellular trap formation, and improves survival in a murine sepsis model. J Innate Immun 2017; 9: 22-32.
[23] Zhang XX, Du ZD, Wen SG and Sun XP. Echocardiographic evaluation of coronary abnormalities and cardiac function in a murine model of kawasaki disease using high-frequency ultrasound. Chin Med J (Engl) 2017; 130: 1467-1474.
[24] Lang RM, Bierig M, Devereux RB, Flachskampf FA, Foster E, Pellikka PA, Picard MH, Roman MJ, Seward J, Shanewise J, Solomon S, Spencer KT, St John Sutton M and Stewart W; American Society of Echocardiography's Nomenclature and Standards Committee; Task Force on Chamber Quantification; American College of Cardiology Echocardiography Committee; American Heart Association; European Association of Echocardiography, European Society of Cardiology. Recommendations for chamber quantification. Eur J Echocardiogr 2006; 7: 79-108.
[25] Kirk JA, Holewinski RJ, Kooij V, Agnetti G, Tunin RS, Witayavanitkul N, De Tombe PP, Gao WD, Van Eyk J and Kass DA. Cardiac resynchronization sensitizes the sarcomere to calcium by reactivating GSK-3β. J Clin Invest 2014; 124: 129-138.
[26] Fert-Bober J, Giles JT, Holewinski RJ, Kirk JA, Uhrigshardt H, Crowgey EL, Andrade F, Bingham CO, Park JK, Halushka MK, Kass DA, Bathon JM and Van Eyk JE. Citrullination of myofilament proteins in heart failure. Cardiovasc Res 2015; 108: 232-242.
[27] Fert-Bober J, Venkatraman V, Hunter CL, Liu R, Crowgey EL, Pandey R, Holewinski RJ, Stotland A, Berman BP and Van Eyk JE. Mapping citrullinated sites in multiple organs of mice using hypercitrullinated library. J Proteome Res 2019; 18: 2270-2278.
[28] Crowgey EL, Matlock A, Venkatraman V, Fert-Bober J and Van Eyk JE. Mapping biological networks from quantitative data-independent acquisition mass spectrometry: data to knowl-

edge pipelines. Methods Mol Biol 2017; 1558: 395-413.
[29] Krasny L, Bland P, Kogata N, Wai P, Howard BA, Natrajan RC and Huang PH. SWATH mass spectrometry as a tool for quantitative profiling of the matrisome. J Proteomics 2018; 189: 11-22.
[30] Ge SX, Jung D and Yao R. ShinyGO: a graphical gene-set enrichment tool for animals and plants. Bioinformatics 2020; 36: 2628-2629.
[31] Abdelaziz AI, Pagel I, Schlegel WP, Kott M, Monti J, Haase H and Morano I. Human atrial myosin light chain 1 expression attenuates heart failure. Adv Exp Med Biol 2005; 565: 283-92; discussion 92, 405-15.
[32] Choo YY, Sakai T, Komatsu S, Ikebe R, Jeffers A, Singh KP, Idell S, Tucker TA and Ikebe M. Calponin 1 contributes to myofibroblast differentiation of human pleural mesothelial cells. Am J Physiol Lung Cell Mol Physiol 2022; 322: L348-L364.
[33] Dixon IMC, Landry NM and Rattan SG. Periostin reexpression in heart disease contributes to cardiac interstitial remodeling by supporting the cardiac myofibroblast phenotype. Adv Exp Med Biol 2019; 1132: 35-41.
[34] Huang L, Li L, Yang T, Li W, Song L, Meng X, Gu Q, Xiong C and He J. Transgelin as a potential target in the reversibility of pulmonary arterial hypertension secondary to congenital heart disease. J Cell Mol Med 2018; 22: 6249-6261.
[35] Razani B, Zhang H, Schulze PC, Schilling JD, Verbsky J, Lodhi IJ, Topkara VK, Feng C, Coleman T, Kovacs A, Kelly DP, Saffitz JE, Dorn GW, Nichols CG and Semenkovich CF. Fatty acid synthase modulates homeostatic responses to myocardial stress. J Biol Chem 2011; 286: 30949-30961.
[36] Lim DS, Roberts R and Marian AJ. Expression profiling of cardiac genes in human hypertrophic cardiomyopathy: insight into the pathogenesis of phenotypes. J Am Coll Cardiol 2001; 38: 1175-1180.
[37] Huntley BK, Heublein DM, Sandberg SM and Burnett JC. Cofilin-1: a possible new biomarker for human heart failure. J Card Fail 2007; 13: S101.
[38] Martinod K, Demers M, Fuchs TA, Wong SL, Brill A, Gallant M, Hu J, Wang Y and Wagner DD. Neutrophil histone modification by peptidylarginine deiminase 4 is critical for deep vein thrombosis in mice. Proc Natl Acad Sci U S A 2013; 110: 8674-8679.
[39] Pianta A, Arvikar SL, Strle K, Drouin EE, Wang Q, Costello CE and Steere AC. Two rheumatoid arthritis-specific autoantigens correlate microbial immunity with autoimmune responses in joints. J Clin Invest 2017; 127: 2946-2956.
[40] Pironti G, Gastaldello S, Rassier DE, Lanner JT, Carlström M, Lund LH, Westerblad H, Yamada T and Andersson DC. Citrullination is linked to reduced Ca^{2+} sensitivity in hearts of a murine model of rheumatoid arthritis. Acta Physiol (Oxf) 2022; 236: e13869.
[41] Matsuo K, Xiang Y, Nakamura H, Masuko K, Yudoh K, Noyori K, Nishioka K, Saito T and Kato T. Identification of novel citrullinated autoantigens of synovium in rheumatoid arthritis using a proteomic approach. Arthritis Res Ther 2006; 8: R175.
[42] De Meyer SF, Suidan GL, Fuchs TA, Monestier M and Wagner DD. Extracellular chromatin is an important mediator of ischemic stroke in mice. Arterioscler Thromb Vasc Biol 2012; 32: 1884-1891.
[43] Savchenko AS, Borissoff JI, Martinod K, De Meyer SF, Gallant M, Erpenbeck L, Brill A, Wang Y and Wagner DD. VWF-mediated leukocyte recruitment with chromatin decondensation by PAD4 increases myocardial ischemia/reperfusion injury in mice. Blood 2014; 123: 141-148.
[44] Fuchs TA, Brill A, Duerschmied D, Schatzberg D, Monestier M, Myers DD, Wrobleski SK, Wakefield TW, Hartwig JH and Wagner DD. Extracellular DNA traps promote thrombosis. Proc Natl Acad Sci U S A 2010; 107: 15880-15885.

Supplementary Materials

Protein digestion using the FASP method for MS-based proteomics

Protein extracts (100 µg) were processed by the FASP protocol using Microcon 30k centrifugal ultrafiltration units (Merck, Darmstadt), and the centrifugation force was 10,000 g according to the manufacturer's instructions. For digestion, LysC (Wako Chemicals, Richmond, VA, USA) in 50 mM Tris HCl buffer was added to each sample at an enzyme-to-protein ratio of 1:60. The samples were incubated at 37°C with no shaking for 3 hr followed by a second dose of LysC at an enzyme-to-protein ratio of 1:60. The released peptides were collected by centrifugation at 10,000 × g for 10 min followed by two washes with 100 µL of 50 mM Tris/HCl (pH 8.5). The peptides in the eluent were assessed by BCA assays. Eluates containing 50 µg of total peptide were acidified by the addition of trifluoroacetic acid (TFA) to a 2% final concentration and desalted on uElution C18 Oasis HLB plates (Waters, Milford, MA, USA), followed by vacuum. The samples were frozen at -80°C until MS-based analysis of total protein quantification and citrullination by DIA-MS.

Hypercitrullinated library sample preparation

Two 100 µg aliquots were used per sample. Protein lysates were processed by the FASP protocol as described previously with some modifications. Briefly, the FASP protocol was carried out until the step of washing the samples with 100 µL of 50 mM Tris/HCl (pH 8.5). Instead of being washed with Tris/HCl, the samples were washed twice with deimination buffer (5 mM DTT, 10 mM $CaCl_2$, 100 mM Tris, pH 7.6). Next, one aliquot of each sample of PAD cocktail solution was added to 60 µL of deamidation buffer (enzyme to protein ratio of 1:25). To the corresponding sample aliquot, water was added at the same volume as the PAD cocktail. The samples were incubated at 37°C for 2 hr. Subsequently, after two washes with 100 µL of 50 mM Tris/HCl (pH 8.5), the samples were digested with LysC as described previously. The eluted peptides were dried on a spread vacuum and fractionated using a High pH Reversed-Phase Peptide fractionation kit (Thermo Scientific™ Pierce™). The fractions were evaporated using vacuum centrifugation and stored at -80°C until they were used for DDA. DDA acquisition was carried out on a TripleTOF 5600+ instrument (AB SCIEX) as described previously with some modifications [27]. Briefly, aliquots containing ~5 µg of peptides were dissolved in buffer A (0.1% FA), spiked with iRT calibration mix (Biognosys AG) and injected and separated on an Eksigent 415 LC system that was operated in microflow mode coupled to a TripleTOF 5600+ mass spectrometer. One microgram of peptides in each sample was preloaded onto the trap column (ChromXP C18CL 10 × 0.3 mm 5 µm 120 Å) at a flow rate of 10 µL/min for 3 min and separated on the analytica l column (ChromXP C18CL 150 × 0.3 mm 3 µm 120 Å) at a flow rate of 5 µL/min using a linear A-B gradient of 2-35% Buffer B (98% ACN, 0.1% FA) for 120 min. In one cycle, one MS1 scan was followed by 20 MS2 scans. The MS1 scan collected 300-1250 m/z for 250 ms, and the MS2 scan collected 100-1,500 m/z for 100 ms. The exclusion time for precursor ion selection was set to 12 s. Ions were fragmented for the MS2 experiment in the collision cell using a collision energy according to the equation of a doubly charged peptide that was ramped ± 15 V from the calculated collision energy.

The DDA MS raw files were analyzed as previously described [27]. Briefly, the DDA raw files (wiff) were converted to centroided mzML files using ProteoWizard v.3.0.6002 and searched through the Trans Proteomics Pipeline (TPP) [1, 2] using the following algorithms: Comet [3]; X!tandem! Native scoring; and X!tandem! K-scoring [4] against a reviewed mouse canonical protein sequence database downloaded from the UniProt database on January 24th, 2022. The precursor and fragment mass tolerances for the search algorithms were set to 10 ppm. Peptide probability modeling was performed using the TPP peptide prophet "xinteract", and the results searches were combined using the TPP "interprophet parser". Further filtering was performed using Mayu to select peptide spectral match probability values that were consistent with a 1% peptide false discovery rate (FDR), and a spectral library was generated using the TPP SpectraST tool. Retention times (RTs) were then normalized to 'indexed' retention time space using the custom Python script spectrast2spectrast_irt.py, which is publicly available via the MSPROTEOMICSTOOLS python package (https://github.com/msproteomicstools/msproteomicstools). Biognosys internal retention time reference peptides were added to each sample immediately before

acquisition and were used for RT alignment. The search parameters were as follows: a maximum of 2 missed cleavages, carbamidomethylation of cysteines set as a fixed modification, and variable modifications of oxidation (M), deamidation (NQ) and citrullination (R). The peptides were filtered at an FDR of 1% with a peptide probability cutoff ≥ 0.99. The raw spectral libraries were generated from the valid peptide spectrum matches and then refined into nonredundant consensus libraries [5] using SpectraST v.4.047 [6]. Modified unmodified pairs of citrullinated peptides were analyzed for physiochemical properties such as delta retention time shift (ΔRT), charge state and neutral loss. Finally, only sites with ≥ 5-minute ΔRT were reported as validated sites.

Data-independent acquisition-MS (DIA-MS) analysis

Peptides derived from tissue samples were dissolved in 0.1% FA containing iRT peptides. The liquid chromatography settings were the same as described for the DDA analysis. The mass spectrometer was operated in SWATH mode [7], and full profile MS1 scans were acquired in the mass range of m/z 300-1500 in positive ion mode. MS1 scans were acquired using a dwell time of 250 ms in a mass range of 400-1250 m/z at 45,000 FWHM. MS2 scans were acquired in high-sensitivity mode at 15,000 FWHM over a precursor range of 400-1250 m/z with an MS2 range of 100-1800 m/z using 100 variable windows with a dwell time of 30 ms. The workflow was performed as previously described [28]. SWATH-MS files were converted to 32-bit profile mzXML files using msconvert (Proteowizard V.3.0.447). OpenSWATH analysis and iRT peptides were used for retention time normalization [8]. The XIC extraction window was 20 min. An extended version of PyProphet [9] was used for FDR estimation. For each tissue dataset, 1% protein FDR at the global level was applied. The peak area of fragment ions was used for peptide quantification. To quantify proteins, the mean value of the peptide quantities was calculated. The protein quantification results were exported as a tsv file and further processed and statistically analyzed with MAPDIA software [10].

[1] Chambers MC, Maclean B, Burke R, Amodei D, Ruderman DL, Neumann S, Gatto L, Fischer B, Pratt B, Egertson J, Hoff K, Kessner D, Tasman N, Shulman N, Frewen B, Baker TA, Brusniak MY, Paulse C, Creasy D, Flashner L, Kani K, Moulding C, Seymour SL, Nuwaysir LM, Lefebvre B, Kuhlmann F, Roark J, Rainer P, Detlev S, Hemenway T, Huhmer A, Langridge J, Connolly B, Chadick T, Holly K, Eckels J, Deutsch EW, Moritz RL, Katz JE, Agus DB, MacCoss M, Tabb DL and Mallick P. A cross-platform toolkit for mass spectrometry and proteomics. Nat Biotechnol 2012; 30: 918-920.

[2] Keller A, Eng J, Zhang N, Li XJ and Aebersold R. A uniform proteomics MS/MS analysis platform utilizing open XML file formats. Mol Syst Biol 2005; 1: 2005.0017.

[3] Eng JK, Jahan TA and Hoopmann MR. Comet: an open-source MS/MS sequence database search tool. Proteomics 2013; 13: 22-24.

[4] Craig R and Beavis RC. TANDEM: matching proteins with tandem mass spectra. Bioinformatics 2004; 20: 1466-1467.

[5] Collins BC, Gillet LC, Rosenberger G, Röst HL, Vichalkovski A, Gstaiger M and Aebersold R. Quantifying protein interaction dynamics by SWATH mass spectrometry: application to the 14-3-3 system. Nat Methods 2013; 10: 1246-1253.

[6] Lam H, Deutsch EW, Eddes JS, Eng JK, Stein SE and Aebersold R. Building consensus spectral libraries for peptide identification in proteomics. Nat Methods 2008; 5: 873-875.

[7] Röst HL, Rosenberger G, Navarro P, Gillet L, Miladinović SM, Schubert OT, Wolski W, Collins BC, Malmström J, Malmström L and Aebersold R. OpenSWATH enables automated, targeted analysis of data-independent acquisition MS data. Nat Biotechnol 2014; 32: 219-223.

[8] Röst HL, Liu Y, D'Agostino G, Zanella M, Navarro P, Rosenberger G, Collins BC, Gillet L, Testa G, Malmström L and Aebersold R. TRIC: an automated alignment strategy for reproducible protein quantification in targeted proteomics. Nat Methods 2016; 13: 777-783.

[9] Röst HL, Aebersold R and Schubert OT. Automated SWATH data analysis using targeted extraction of ion chromatograms. Methods Mol Biol 2017; 1550: 289-307.

[10] Teo G, Kim S, Tsou CC, Collins B, Gingras AC, Nesvizhskii AI and Choi H. mapDIA: preprocessing and statistical analysis of quantitative proteomics data from data independent acquisition mass spectrometry. J Proteomics 2015; 129: 108-120.

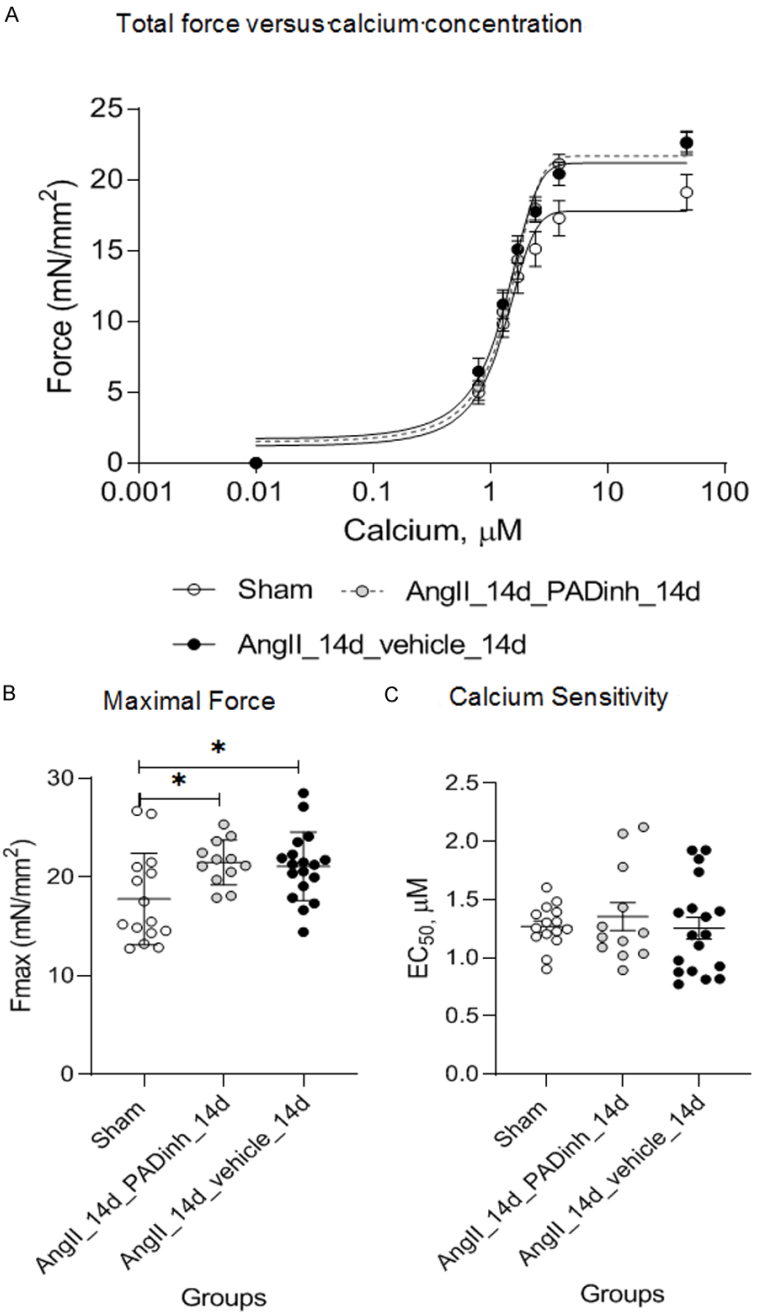

Supplementary Figure 1. Myofilament function is reduced in the AngII model. (A) Mean force as a function of calcium concentration (± SEM) and the fitted curves of skinned myocytes from the LV lateral wall in the Sham, AngII_14d, AngII_14d_PADinh_14d and AngII_14d_vehicle_14d groups. Summary results of the (B) Fmax and (C) EC50 of these curve fits are shown as individual myocytes and the mean ± SEM (n=3-6 hearts, n-=3 myocytes per heart), *P < 0.05, **P < 0.01.

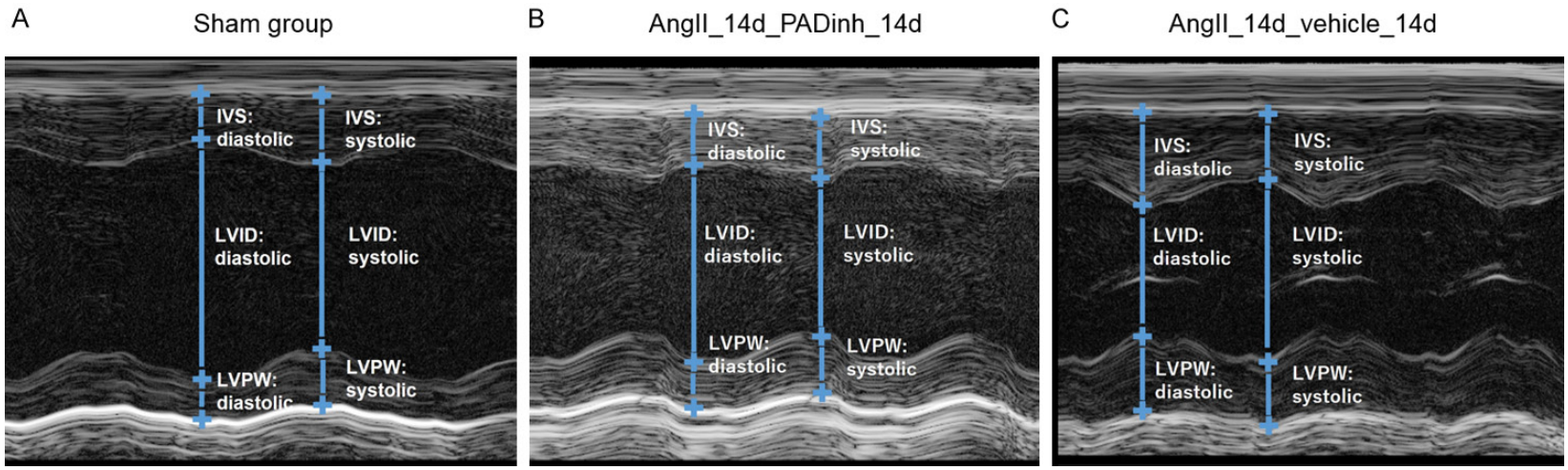

Supplementary Figure 2. Effects of PAD inhibitor on cardiac function evaluated by conventional echocardiography. Representative M-mode images of Sham group (A), AngII_14d_PAD-inh_14d (B), and AngII_14d_vehicle_14d (C).